



RESEARCH ARTICLE

10.1002/2017JA024713

Key Points:

- Multipoint Swarm 50 sps magnetic field data reveal unexpectedly large amplitude time-varying fields which evolve on 10 s timescales
- The observed E - and B -field spectra are consistent with a continuum of incident, reflected, and interfering Alfvén waves
- Alfvén wave dynamics are shown to be of fundamental importance for magnetosphere-ionosphere coupling and consistent with an IAR model

Correspondence to:

I. P. Pakhotin,
i.p.pakhotin@gmail.com

Citation:

Pakhotin, I. P., Mann, I. R., Lysak, R. L., Knudsen, D. J., Gjerloev, J. W., Rae, I. J., ... Balasis, G. (2018). Diagnosing the role of Alfvén waves in magnetosphere-ionosphere coupling: Swarm observations of large amplitude nonstationary magnetic perturbations during an interval of northward IMF. *Journal of Geophysical Research: Space Physics*, 123. <https://doi.org/10.1002/2017JA024713>

Received 26 AUG 2017

Accepted 28 DEC 2017

Accepted article online 3 JAN 2018

Diagnosing the Role of Alfvén Waves in Magnetosphere-Ionosphere Coupling: Swarm Observations of Large Amplitude Nonstationary Magnetic Perturbations During an Interval of Northward IMF

I. P. Pakhotin¹ , I. R. Mann¹ , R. L. Lysak² , D. J. Knudsen³ , J. W. Gjerloev⁴ , I. J. Rae⁵ , C. Forsyth⁵ , K. R. Murphy⁶ , D. M. Miles^{1,7} , L. G. Ozeke¹ , and G. Balasis⁸

¹Department of Physics, University of Alberta, Edmonton, Alberta, Canada, ²School of Physics and Astronomy, University of Minnesota, Minneapolis, MN, USA, ³University of Calgary, Calgary, Alberta, Canada, ⁴Johns Hopkins University Applied Physics Laboratory, Laurel, MD, USA, ⁵Mullard Space Science Laboratory, University College London, London, UK, ⁶NASA Goddard Space Flight Center, Greenbelt, MD, USA, ⁷Department of Physics and Astronomy, University of Iowa, Iowa City, IA, USA, ⁸National Observatory of Athens, Athens, Greece

Abstract High-resolution multispacecraft Swarm data are used to examine magnetosphere-ionosphere coupling during a period of northward interplanetary magnetic field (IMF) on 31 May 2014. The observations reveal a prevalence of unexpectedly large amplitude (>100 nT) and time-varying magnetic perturbations during the polar passes, with especially large amplitude magnetic perturbations being associated with large-scale downward field-aligned currents. Differences between the magnetic field measurements sampled at 50 Hz from Swarm A and C, approximately 10 s apart along track, and the correspondence between the observed electric and magnetic fields at 16 samples per second, provide significant evidence for an important role for Alfvén waves in magnetosphere-ionosphere coupling even during northward IMF conditions. Spectral comparison between the wave E - and B -fields reveals a frequency-dependent phase difference and amplitude ratio consistent with interference between incident and reflected Alfvén waves. At low frequencies, the E/B ratio is in phase with an amplitude determined by the Pedersen conductance. At higher frequencies, the amplitude and phase change as a function of frequency in good agreement with an ionospheric Alfvén resonator model including Pedersen conductance effects. Indeed, within this Alfvén wave incidence, reflection, and interference paradigm, even quasi-static field-aligned currents might be reasonably interpreted as very low frequency ($\omega \rightarrow 0$) Alfvén waves. Overall, our results not only indicate the importance of Alfvén waves for magnetosphere-ionosphere coupling but also demonstrate a method for using Swarm data for the innovative experimental diagnosis of Pedersen conductance from low-Earth orbit satellite measurements.

Plain Language Summary The study shows evidence that electromagnetic waves in the ionosphere and currents flowing into the ionosphere can be described by the same physical model. This is important for estimating the total energy going into the ionosphere and potentially allows deriving important high-resolution information about the ionosphere by studying data recorded when spacecraft fly over the auroral region.

1. Introduction

Field-aligned currents (FACs) flowing between the magnetosphere and the ionosphere provide the basis for the transfer of energy and momentum between the two systems (e.g., Cowley, 2000; Foster et al., 1983; Lu et al., 1998). On the largest scale, FACs form the Region 1 and Region 2 current systems (Iijima & Potemra, 1976, 1978). However, currents across a range of scales are important in magnetosphere-ionosphere coupling (e.g., Hasunuma et al., 2008; Peria et al., 2000; Rother et al., 2007). FACs are usually inferred from in situ satellite magnetic field data. Under the assumption that the FACs consist of long current sheets orientated perpendicular to the spacecraft orbit, FACs can be calculated from the observed transverse magnetic field variation via Ampère's law, neglecting the displacement current (e.g., Ritter et al., 2013, and references therein). Significantly, this single-spacecraft approach must assume that all the transverse magnetic oscillations occur as the result of spacecraft motion through static and infinite current sheets. Any temporal variations in the magnetic field during the crossing of a FAC element will result in a violation of this

©2018. The Authors.

This is an open access article under the terms of the Creative Commons Attribution License, which permits use, distribution and reproduction in any medium, provided the original work is properly cited.

assumption. As a consequence, errors are introduced into the inferred FAC estimates as a result of the misinterpretation of temporal variations, such as might be associated with Alfvén waves, as spatial structures associated the FACs (see e.g., Forsyth et al., 2017, and references therein).

Various techniques have been devised to assess and try to overcome the potential stationarity problem in FAC estimation. Using multispacecraft ST-5 measurements, Gjerloev et al. (2011) determined that FAC systems with scale sizes larger than ~ 200 km were stable and quasi-persistent on timescales of the order of a minute, comparable to a LEO satellite's traversal time across the auroral zone. For the European Space agency (ESA) Swarm mission, a dual-spacecraft FAC estimation methodology based on a path integration using two "side-by-side" spacecraft has also been developed (Ritter et al., 2013). In this dual spacecraft technique, data from the "side-by-side" Swarm A and C spacecraft are low-pass filtered to ensure that only currents with spatial scale lengths $> \sim 150$ km are represented. The validity of the low-pass filtering used to produce such FAC estimates relies on the hypothesis that the role of these smaller scale structures can be neglected in comparison to those arising from the larger scale FACs. For example, Lühr et al. (2015) used statistical analysis to separate these magnetic disturbances into small-scale structures (< 10 km) which they related to Alfvén waves and large-scale quasi-stationary FACs (> 150 km). Unfortunately, the low-pass filtering approach has the effect of excluding information about any potential impacts arising from small-scale FACs (e.g., Miles et al., 2016, Figure 19) and precludes an investigation of the potential importance of nonstationary processes such as Alfvén wave effects in driving magnetosphere-ionosphere coupling, not only on scales < 10 km but also in the range of 10–150 km.

Multispacecraft measurements from relatively closely spaced satellites with near coaligned orbits can also be used to assess nonstationarity and to infer whether the observed magnetic disturbances are quasi-static on the timescale of the spacecraft separation (see e.g., Forsyth et al., 2017). Depending on orbital orientations, and cross- and along-track separations, it is also possible that interspacecraft variations can also occur due to the currents being localized in azimuth, or due to the FACs changing intensity on the timescale of the along-track temporal separation (cf. Forsyth et al., 2017). Care must be therefore taken to assess such effects. However, using simultaneous electric- and magnetic-field measurements, where available, it is possible to better elucidate whether any given structure is static or Alfvénic in nature. This also provides the means to investigate the role of Alfvén waves in the electrodynamics of MIC under various solar wind driving conditions, and we use the combination of Swarm electric and magnetic field data to examine that here.

This study presents Swarm dual-spacecraft analysis of an FAC crossing during quiet northward interplanetary magnetic field (IMF) conditions. Regions of apparently nontime-stationary magnetic field variations are observed in a single pass, even though the interspacecraft separation between Swarm A and C is only around 10 s along track and 1.4° cross track. Simultaneous E -field and B -field measurements on Swarm A are carried out for the same interval to evaluate the impact of Alfvén waves at various scale sizes.

2. Data and Methodology

During the time period under study, the Swarm A and C satellites (Friis-Christensen et al., 2008) were in a near-polar low-Earth orbit (LEO) at 450 km altitude, separated by 1.4° azimuthally, corresponding to a cross-track separation of around 120 km at the equator, and approximately 10 s separation along track. During the event under study this corresponds to separations of ~ 8 –50 km cross track and ~ 75 km along track. The Swarm spacecraft are equipped with vector fluxgate magnetometers sampling at 50 vectors per second (Friis-Christensen et al., 2008). The spacecraft also carry the Electric Field Instrument which consists of the Thermal Ion Imager (TII) and the Langmuir Probe (Knudsen et al., 2017). The TII measures ion velocity moments at up to 16 vectors/s which can be converted into electric field measurements using an assumed frozen-in condition at Swarm altitudes such that $\mathbf{E} = -\mathbf{v} \times \mathbf{B}$, where \mathbf{v} is the ion velocity inferred from the TII ion moments and \mathbf{B} is the magnetic field.

The local electrodynamics at Swarm can also be interpreted in the context of the larger scale field aligned currents associated with global convection by comparing them with data from the Active Magnetosphere and Planetary Electrodynamics Response Experiment (AMPERE) (e.g., Anderson et al., 2002; Anderson, Takahashi, & Toth, 2000; Green et al., 2006; Murphy et al., 2012; Murphy et al., 2013; Waters et al., 2001). AMPERE uses data from the engineering magnetometers on the Iridium satellite constellation to derive vertical current maps. The Iridium magnetometers have data resolution of 48 nT with data consisting of

observations from >70 satellites in six orbital planes used to produce global current maps. The recurrence time for satellites in each orbital plane is ~10 min; each map is produced under an assumption of quasi-stationarity on a timescale of ~10 min. The maps are updated globally with a 2 min cadence. AMPERE data are used in this study to provide large scale background FAC context for the detailed analysis of the related electrodynamics which are probed using data from the Swarm A and C satellites, which, as described above, are much more closely separated along track (~10s) than those in the Iridium constellation (~10 min).

The CARISMA array (Mann et al., 2008) is a Canada-wide network of fluxgate (FGM) and induction coil (ICM) magnetometers measuring magnetic field perturbations with up to 8 Hz sampling rate for the FGMs and up to 100 Hz for the ICMs. Some of these stations are close to the flight path of Swarm in this study and provide a useful ground check on any observed in situ magnetic pulsations.

3. Results

The study focuses on an auroral zone crossing between 17:16 and 17:22 UT on 31 May 2014. The geomagnetic conditions (King & Papitashvili, 2005) in the hours preceding the Swarm auroral zone crossing, indicated by the red lines, are shown in Figure 1. Figures 1a(i), 1a(ii), and 1a(iii) show the x , y , and z GSM components of the interplanetary magnetic field (IMF). Figures 1a(iv) and 1a(v) show the SYM-H and AE activity indices, and the bottom shows the solar wind dynamic pressure. The IMF and solar wind conditions have been lagged to the magnetopause. The IMF B_z (Figure 1a(iii)) was positive for at least 5 h before the crossing, suggesting that the polar cap should be almost completely closed at this time (e.g., Newell et al., 1997). The AE index (Figure 1a(v)) and SYM-H (Figure 1a(iv)) show relatively quiet conditions, while the dynamic pressure (Figure 1a(vi)) remained above 2 nPa throughout, although showed some small fluctuations during and immediately preceding the pass. The AMPERE-derived FAC map for 17:16–17:18 UT is shown in Figure 1b. The large-scale FACs are quasi-static, largely confined to high latitudes, and rather irregular. In particular, there is a lack of the signature of the classic concentric rings of the Region 1 and Region 2 current systems, as expected for a northward IMF period (e.g., Hoffman et al., 1988). It can be seen from Figure 1 that the Swarm A/C spacecraft pair was on a poleward trajectory up to 17:17 UT followed by an equatorward pass in the ~03–08 MLT sector, initially crossing an extended but rather weak FAC region up to around 17:18 UT, associated according to AMPERE with perhaps weakly upward FAC, before entering a region more clearly characterized by AMPERE as a region of downward FACs (blue).

The Fort Simpson (FSIM) ground magnetometer data from the Canadian Array for Real-time Investigations of Magnetic Activity (CARISMA; Mann et al., 2008) are close to the location Swarm A and C overpass during the time period under study. Data from the 8 Hz FSIM fluxgate magnetometer (FGM) are displayed on Figure 1c. It can be seen that at the time of the crossing the FSIM ground observations show only small perturbations of the order of several nanotesla. Generally throughout the day the station mainly sees variations due to the solar quiet current system, with some at most modest magnetic local midnight activity earlier in the UT day at this station. These quiescent conditions represent typical magnitudes observed by ground magnetometers during very quiet periods characterized by northward IMF.

Swarm A and C magnetic field data in mean-field aligned (MFA) coordinates are displayed in the top panel of Figure 2. The mean field was derived by taking a running average over a 40 s window. The three components in the orthogonal MFA coordinate system then correspond to a vector along the mean magnetic field (MFA_3), a horizontal vector pointing toward the geomagnetic east (MFA_2), and MFA_1 completing the triad pointing approximately in the magnetic north-south direction. The data from Swarm C has been lagged with respect to Swarm A by 10.66 s, corresponding to a lag which maximizes correlation between the time series. This time lag helps compensate for interspacecraft along-track separation and any angle-of-attack effects. Despite the very quiet geomagnetic conditions, there are large magnetic perturbations in the two transverse components reaching tens to hundreds of nT. This is in stark contrast to the apparent small amplitudes seen on the ground. Given the temporal scales of the magnetic signals in the Swarm frame, such a disparity could result from these small-scale disturbances being largely screened from the ground by Biot-Savart integration. Significantly, however, from the perspective of, for example, statistical analyses of Swarm data, the small amplitudes and quiet conditions seen on the ground and which would also be reflected in low magnitudes of local and likely planetary range indices such as K and K_p derived from ground-based magnetometer data cannot be used to conclude that the magnetic perturbations at Swarm altitudes are also small.

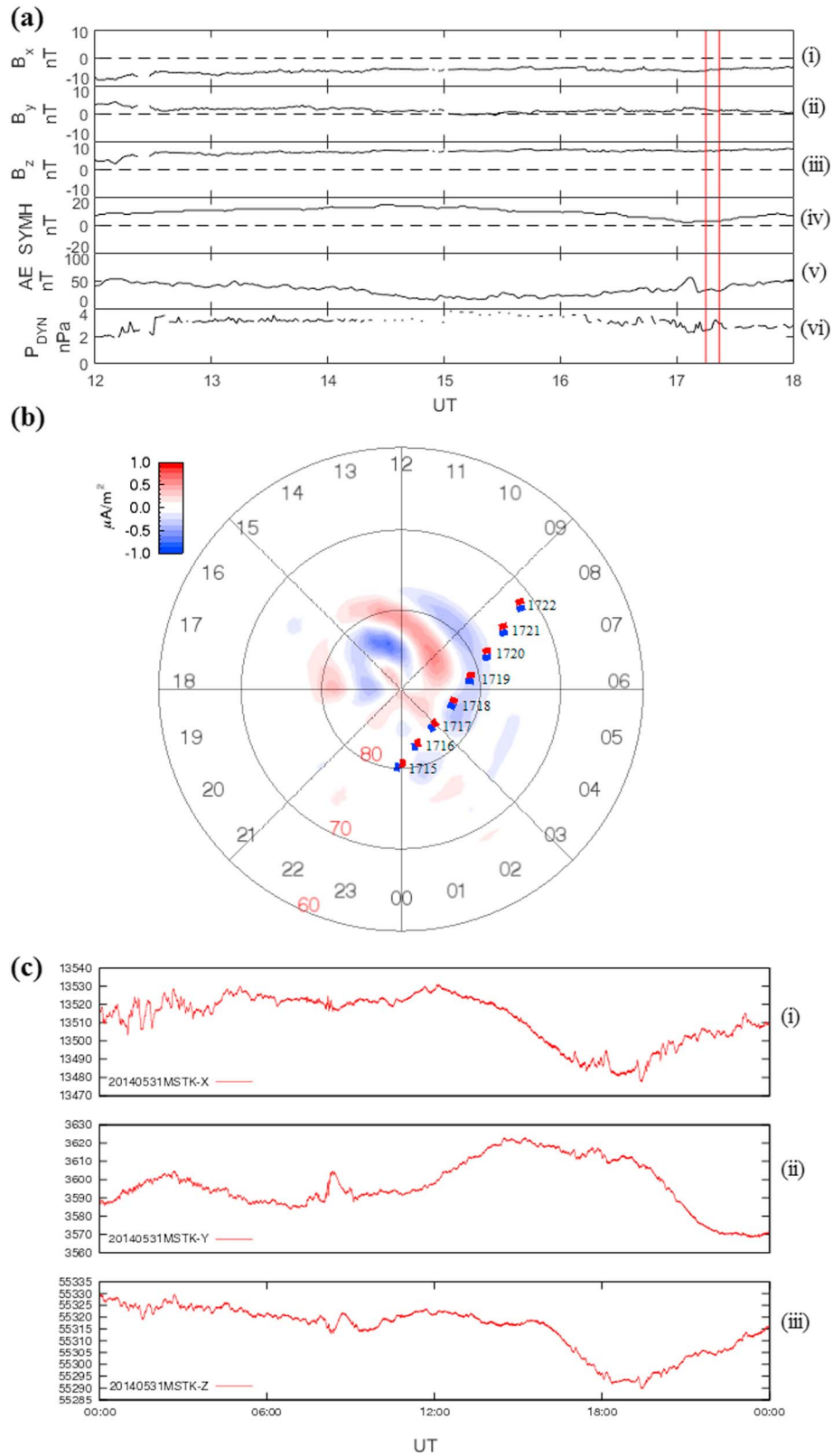


Figure 1. (a) (top to bottom): (i) IMF B_x (GSM), (ii) IMF B_y (GSM), (iii) IMF B_z (GSM), (iv) SYM-H, (v) AE index, and (vi) solar wind dynamic pressure. The red vertical bars denote the interval under study. (b) AMPERE FAC map for 17:16–17:18 UT overplotted with Swarm A (blue) and C (red) spacecraft tracks, with locations labeled in UT. The red and black numbers denote AACGM latitude and MLT. The red and blue colors on the FAC map denote upward and downward FACs, respectively. (c) FSIM CARISMA FGM time series for the time of the pass: (top) north-south, (middle) east-west, and (bottom) up-down components.

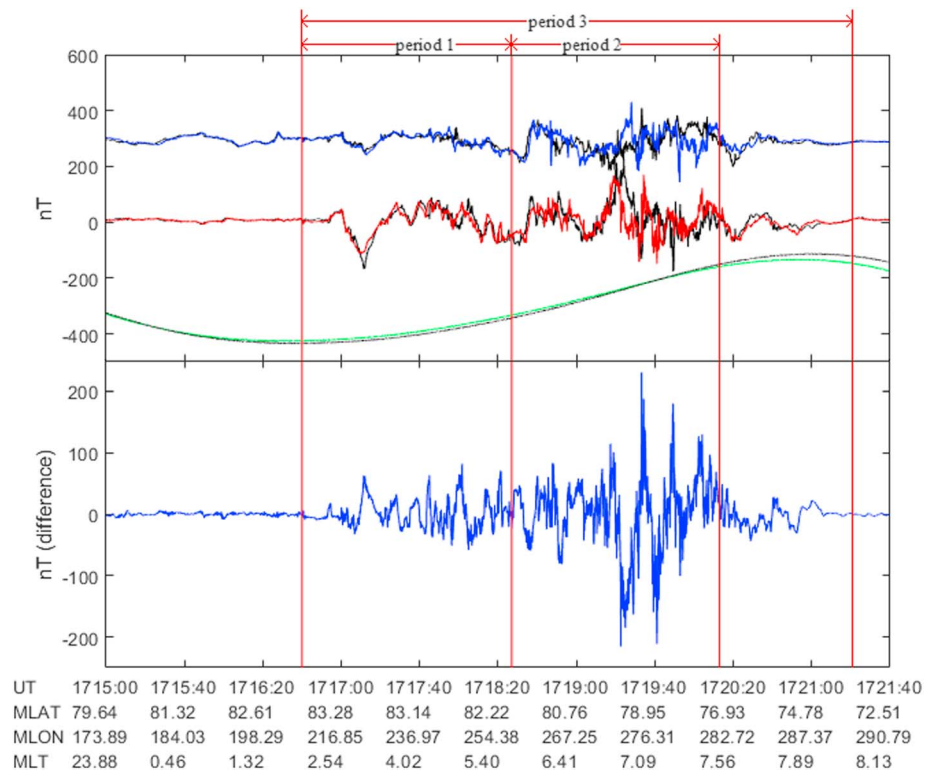


Figure 2. (top) Vector magnetic field observed Swarm A and C: MFA_1 (north-south; blue/black; offset by +300 nT), MFA_2 (east-west) in red/black, and MFA_3 (compressional; offset by -300 nT after mean removal, green/black). Note the much smaller amplitude perturbations in the compressional compared to the transverse components. All components of the Swarm C time series have been lagged by 10.66 s. (bottom) The difference arising from subtracting the two MFA_2 components on Swarm A and (lagged by 10.66 s) Swarm C. The red bars show time periods marked for E - B study (below). In this figure and others the x axes are “UT” (hhmm:ss), while “MLAT,” “MLON,” and “MLT” refer to the AACGM magnetic latitude, AACGM magnetic longitude, and magnetic local time, respectively.

Figure 2 shows that the transverse perturbations are fairly well correlated between the Swarm A and lagged Swarm C data between 17:16:40 and 17:18:27 UT. The agreement is particularly clear in the MFA_2 component (correlation coefficient $R = 0.8920$). However, after 17:18:27 UT the agreement between the two time series and the magnetic signatures drops ($R = 0.4548$ between 17:18:27 and 17:20:13) even though the two spacecraft are only ~ 10 s apart along track. Then, after about 17:19:42 UT, coherency between the two time series increases again as the satellites exit the FAC region.

The morphology observed in this Swarm pass very much resembles the “static” and “Alfvénic” regions denoted in Figure 3 of Ohtani et al. (1996), where conjugate Viking and DMSP-F7 satellites traversed a region of Birkeland currents one after the other. However, the distinction between the “static” and “Alfvénic” regions in the Viking and DMSP-F7 data was made based on the basis of ~ 15 min along-track separations as well as from two platforms at significantly different altitudes. In contrast, in the case of Swarm A and C, the spacecraft are at the same altitude and separated by only around 10 s along track.

To illustrate the magnitude of the change in magnetic field, Figure 2 (bottom) shows the residual created by subtracting the lagged MFA_2 magnetic field components observed by Swarm A from that from Swarm C. It can be seen that the residual between the two appropriately lagged time series is low in the early part of the pass (range = 139.8 nT, root-mean-square (RMS) = 15.9638 between 17:16:40 and 17:18:27 UT). As the spacecraft move equatorward, the differences steadily increase (range = 446.1 nT, RMS = 57.3203 nT between 17:18:27 and 17:20:13 UT), exhibiting multiple >100 nT perturbations in this time period. Meanwhile, the ranges of the constituent MFA_2 time series on Swarm A during these two periods increase from 193.9 nT to 318.5 nT. Therefore, the range of the residual is below the range of constituent quasi-stationary magnetic field perturbations in Period 1, but in Period 2, the range of the residual exceeds the range of presumably

Alfvénic perturbations. The area of poor correlation appears to coincide with a region of net downward FAC as seen on AMPERE (see Figure 1b). Correlation for this period does not significantly improve when using different time lags. This suggests either the existence of fine-scale current structures, with scales smaller than the cross-track separation of the Swarm A/C pair, and/or that the magnetic field changes significantly even on the very short 10 s interspacecraft along-track separation timescale. We propose that the latter occurs as a result of rapid temporal variations caused by large amplitude Alfvén waves and examine this further below.

We use the available data from the TII on Swarm A to derive electric fields and examine the nature of the electromagnetic dynamics of the disturbances. Figure 3a shows the detrended cross-track component of the magnetic field observed by Swarm A together with the cross-track component of the ion moment. This latter measurement is derived from the location of the centroid (moment) of the distribution of particles impacting the detector plate in the TII instrument—a cross-track ion velocity component changes the direction of arrival of the incident rammed ion signal, displacing it in azimuthal angle on the detector. As such, the ion moment is a zero-order measurement from which ion velocity and electric field are later derived (Knudsen et al., 2017). This parameter is plotted here to demonstrate clearly that the correspondence between these independent measurements is not an artifact of any processing but is representative of a physical relationship between the ion flows and the magnetic perturbations. It can be seen that there is truly remarkable correspondence at multiple scales in the frame of Swarm A between the independent measurements of the magnetic perturbations and the ion moment measurements corresponding to ion velocity. The electric field can be calculated from ion velocity distributions under the assumption that the (oxygen) ions are frozen-in at Swarm altitudes such that $\mathbf{E} = -\mathbf{v} \times \mathbf{B}$ (Knudsen et al., 2017). The magnetic field (NEC_2 component) and electric field (NEC_1 component) are plotted on Figure 3b, with NEC being the north-east-center coordinate system with the axes pointing toward geographic north, geographic east, and the center of the Earth, respectively. As with ion velocity, we observe good correspondence between the orthogonal electric and magnetic field components for both large and fine scales. As we demonstrate below, the frequency dependence of this relationship points not only to the importance of the ionospheric Pedersen conductance in controlling the MIC electrodynamics at Swarm altitudes but also to the significance of Alfvén wave incidence, reflection, and interference.

Closer to the ionospheric boundary than one field-aligned Alfvén wavelength, the orthogonal transverse electric and magnetic fields are expected to be well correlated with no phase difference and with the ratio of magnitudes equal to the ionospheric Pedersen conductance (e.g., Lysak, 1991). Well-correlated E - and B -fields are observed in Figure 3f for longer-period perturbations with frequencies in the frame of Swarm <1 Hz. Remembering that changes in FACs are caused by the propagation of Alfvén waves (e.g., Woodroffe & Lysak, 2012; Wright, 1996), this condition is of course also true for quasi-static FAC systems where the timescale of FAC evolution is slow enough such that the same condition is met. Therefore, similarly for static FAC systems, the ratio of magnetic and electric fields close to the current closure location in the ionosphere should also be controlled by an identical boundary condition (e.g., Ishii et al., 1992; Sugiura et al., 1982). In both cases the in-phase relationship is consistent with the requirement for the Poynting flux to be carried from just above the ionosphere into the dissipative ionosphere region below. In the case of Alfvén waves above the reflection point, the amplitude and phase of the magnetic and electric fields will change as a function of the distance along the field line in units of parallel wavelength, due to the superposition of the incident and reflected waves. Such superposition can occur as a result of a single reflection at the ionosphere (e.g., Knudsen, Kelley, & Vickrey, 1992) or the action of the Ionospheric Alfvén Resonator or IAR (Lysak, 1991). In the case of the IAR, where there is an additional reflection from Alfvén speed gradients at high altitudes (typically assumed to lie at altitudes of around 4,000 km), similar structure can develop but on parallel wavelength scales determined by the harmonics of the cavity of the resonator (e.g., Lysak, 1991; Lysak & Song, 2008).

In the frame of Swarm A, the perturbations in these fields can correspond to either a spatial structure of a given scale crossed at the orbital speed of the satellite, a temporal variation, or a combination of the two. In Figures 2 and 3, the large-scale dB/dt corresponding to FACs crossed on timescales of $>\sim 30$ s appear to have good correspondence, in line with the statistical results of Gjerloev et al. (2011), Lühr et al. (2015), and Forsyth et al. (2017) that show FAC with scales >150 – 200 km are in general rather stable. In order to determine whether the reflected Alfvén wave paradigm is applicable to our event, we use synchronous

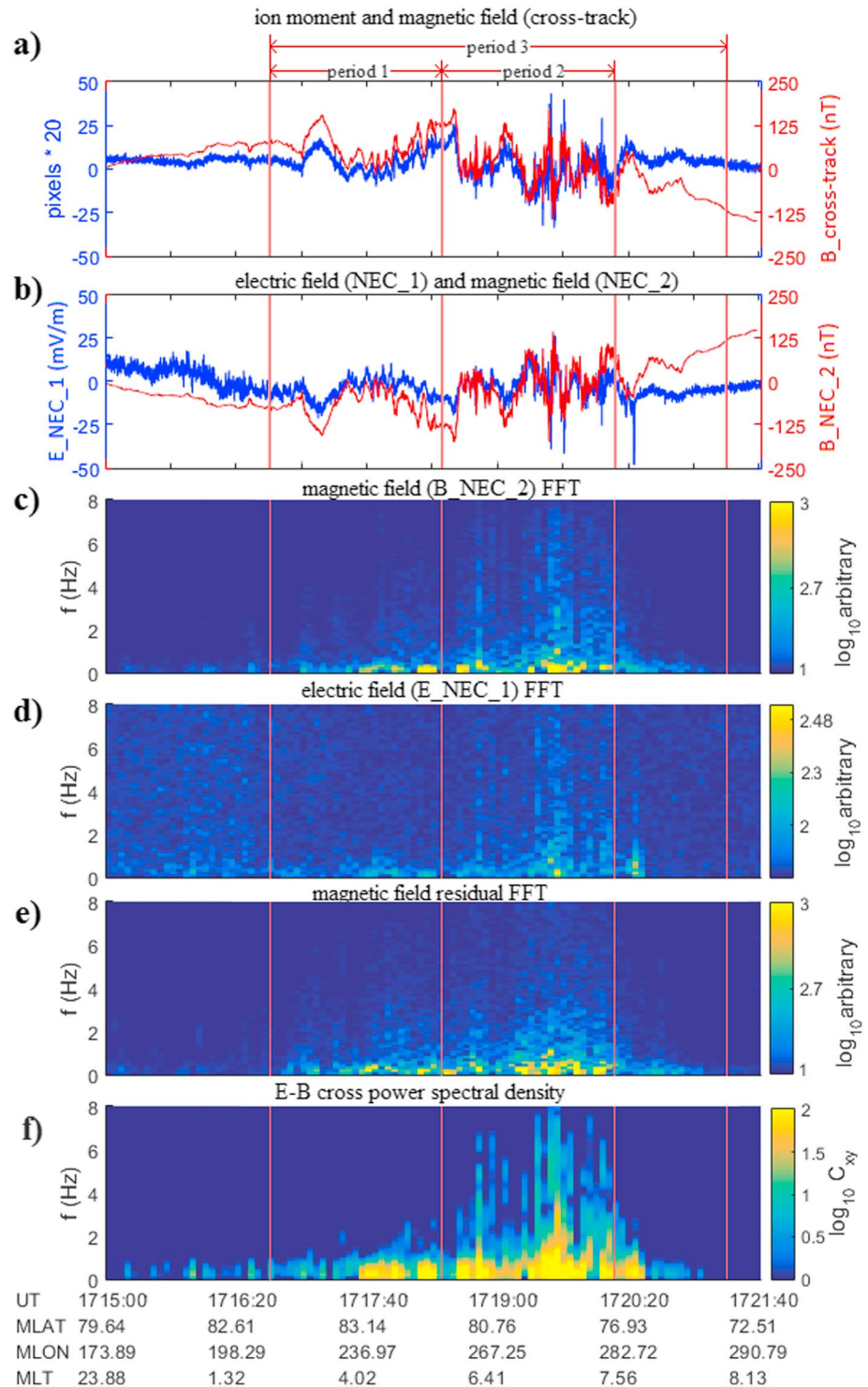


Figure 3. (a) Swarm A linearly detrended cross-track magnetic field (red) and linearly detrended cross-track ion moment (blue, scale derived from the centroid of the TII ion distribution in scaled instrument pixel units), (b) linearly detrended Swarm A NEC_2 magnetic field component (red) and linearly detrended NEC_1 electric field component (blue), (c) the dynamic power spectrum of the red curve in Figure 3b, (d) the dynamic power spectrum of the blue curve in Figure 3b, (e) the dynamic power spectrum of the residual of the 2 MFA_2 magnetic field components from Figure 2 (bottom), and (f) the cross-power spectral density of the magnetic and electric fields from Figure 3b.

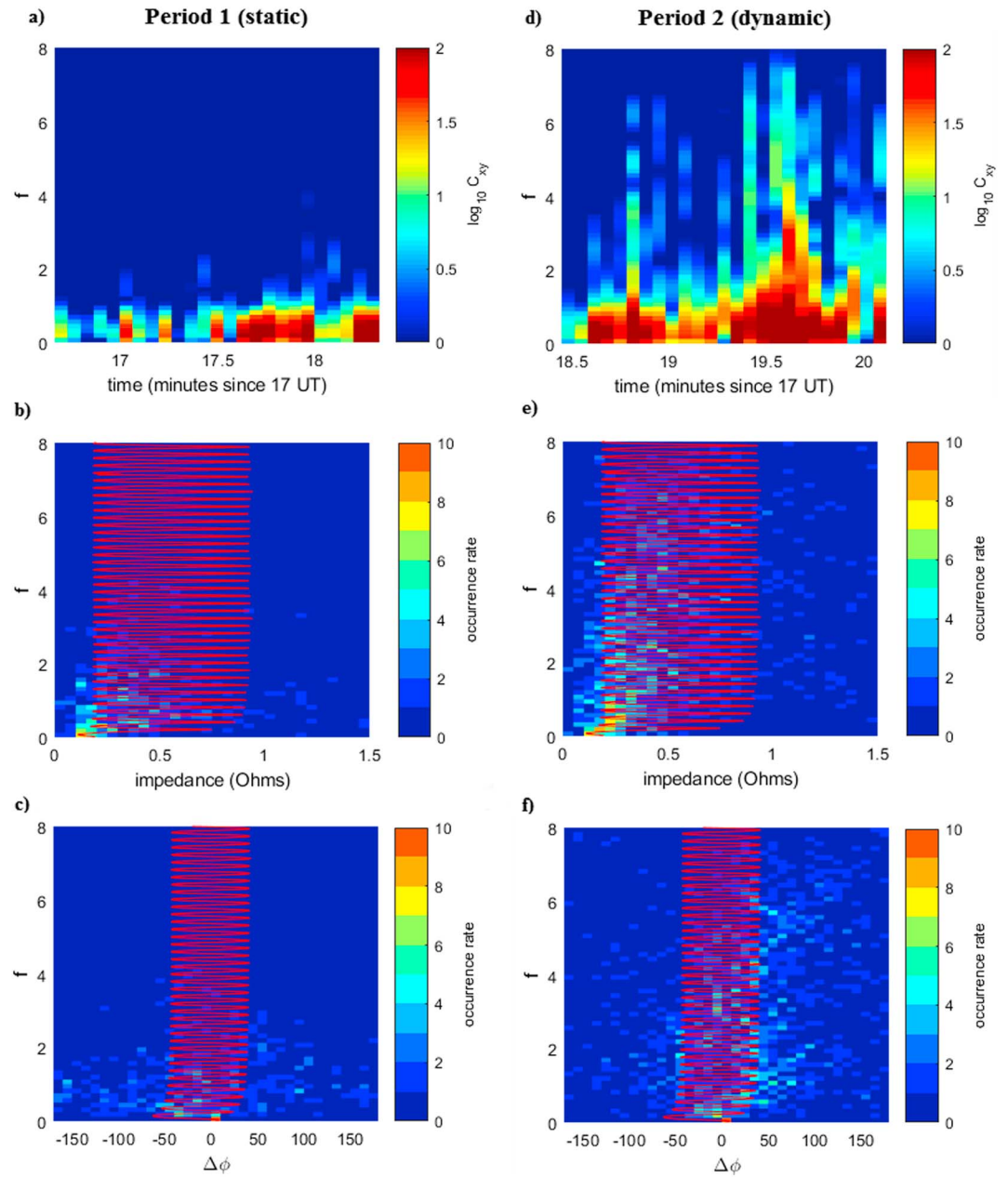


Figure 4. (a and d) Cross-power spectral density, (b and e) impedance histogram, and (c and f) phase difference histogram for periods 1 and 2, respectively. The red curves plotted over the histograms denote the results from the Lysak (1991) IAR model initialized with parameters $V_{ai} = 70$ km/s, $\Sigma P = 5$ S, scale height = 110 km, and altitude above the reflection layer $z = 340$ km. In Figures 4 and 5 “occurrence rate” refers to the total number of spectral points in that frequency and impedance/phase bin that exist in the spectral matrices for that time period and which have survived the thresholding procedure.

measurements of the electric and magnetic fields on Swarm A to empirically determine the frequency-dependent E - B phase and impedance functions (cf. Knudsen et al., 1990; Lysak, 1991).

The dynamic spectra of E (NEC_1) and B (NEC_2) were calculated using a 12.5 s sliding window fast Fourier transform with a 50% overlap. The absolute cross-power spectral density was also calculated, and all elements with a cross-coherence below a threshold of unity were discarded. This was found to represent a good balance between maintaining reasonable statistics and removing low amplitude noise. Of the surviving elements in both matrices, phases were calculated for each complex spectral element in each matrix. The

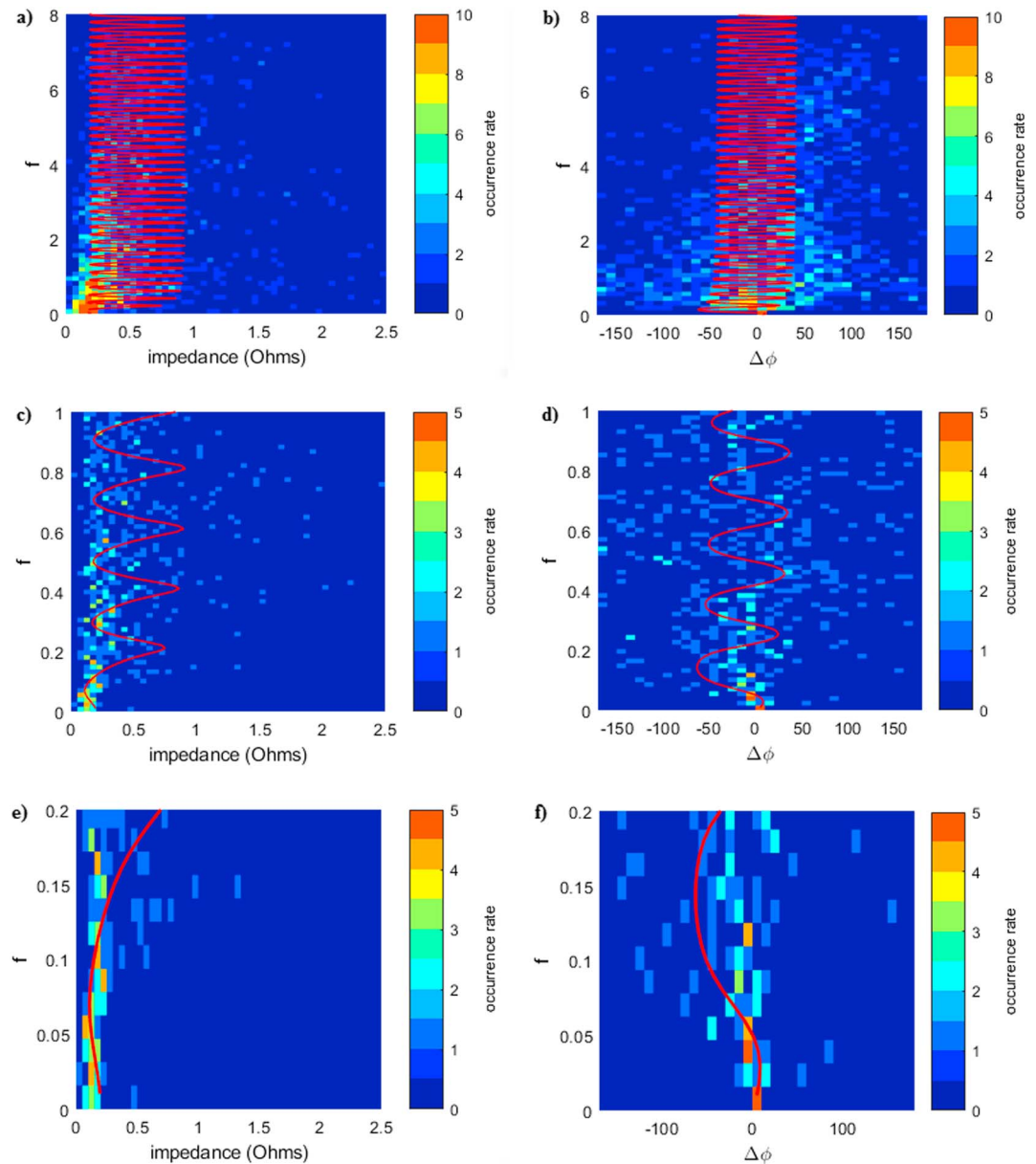


Figure 5. Period 3 (a) impedance and (b) phase calculated using an 8 s window showing frequencies from 0 to 8 Hz. Period 3 impedance and phase calculated using a 64 s window (c and d) for 0–1 Hz and (e and f) for 0–0.2 Hz. The red curves denote the impedance and phase functions from the same model as was applied to Figure 4.

phases were subtracted elementwise to get an *E-B* phase difference matrix. After Grzesiak (2000), a histogram of the occurrence of each phase difference as a function of frequency was calculated. A histogram of impedance was also calculated from the element-wise *E/B* ratio (Ishii et al., 1992; Knudsen et al., 1992) from the absolute magnitudes of the Fourier transforms of the orthogonal transverse components, as per equation (19) in Knudsen et al. (1992):

$$Z(f) = \mu_0 | \sim E_x(f) / \delta \sim B_y(f) |$$

where μ_0 is the magnetic constant, $\sim E_x(f)$ is the Fourier transform of the NEC_1 electric field, and $\delta \sim B_y(f)$ is the Fourier transform of the NEC_2 magnetic field.

The results are shown in Figure 4 for two time periods which are also marked on Figures 2 and 3. The “quasi-static” Period 1, 17:16:40–17:18:27 UT, shows high levels of correspondence between Swarm A

and Swarm C, with residuals never exceeding ± 100 nT. The “dynamic” Period 2, at 17:18:27–17:20:13 UT, features high nonstationarity and residuals exceeding ± 100 nT on several occasions. Both the “quasi-static” and “dynamic” intervals, there is a clear indication of cross power which peaks at low frequencies below 2 Hz, but which also reaches much higher frequencies during the interval of nonstationarity in Period 2 (Figure 3f).

During the first period, the coherent signal (where the cross power is highest) is mostly below 1 Hz (Figure 4a). The impedance histogram (Figure 4b) shows high concentrations of data points at low frequencies, in agreement with time series information. There is a sharp drop in occurrence rate above 1 Hz, as the period is dominated by low frequency fluctuations. The data points above 1 Hz are composed of mostly noise which has low coherency between E_{NEC_1} and B_{NEC_2} , so their points do not reach the aforementioned coherency threshold. The histogram shows clustering around 0.2–0.4 Ω . There is a sharp cutoff at 0.2 Ω below which very few data points exist. There is no such cutoff higher than 0.4 Ω , but rather a gradual decline in occurrence rate for higher impedances. Meanwhile, the phase difference histogram between E and B for Period 1 (Figure 4c) shows that at the lowest frequencies it is concentrated near 0° but spreads rapidly with rising frequencies, mostly populating the parameter space for phase differences between $\sim +90^\circ$ and -90° . There are also a few spectral points which appear to lie above 90° or below -90° . For frequencies < 1 Hz, which dominate this interval, the phase difference is preferentially clustered around 0° . In the north-east-center (NEC) coordinate system used here, phase differences of -90° to $+90^\circ$ signify downgoing Poynting flux. A model for mutually interfering Alfvén waves inside the IAR, derived from the Lysak (1991) methodology, is overplotted in pink for both the impedance and the phase difference histograms. The parameters and assumptions used in the model will be expanded on later in this paper.

The results for Period 2, characterized by large residuals in Figure 2 (bottom), are shown in Figure 4 (Figures 4d–4f for cross-power spectral density, impedance, and phase difference, respectively). During this time, the E - B cross power extends to higher frequencies above 1 Hz up to around 3 Hz or more. The impedance and phase histograms (Figures 4e and 4f) appear qualitatively very similar to those for Period 1 below 1 Hz but also extending the same phase characteristics to higher frequencies. It can be seen that there is more coherent high-frequency content (Figure 4d) which explains the increase in data points at higher frequencies in the histograms.

Period 3 shown in Figure 5 encompasses the entire auroral crossing including Periods 1 and 2. The histograms are calculated after applying two different window lengths. For Figures 5a and 5b the same window applied in Figure 4 is used, which is 8 s, with a 50% overlap between successive windows. Figures 5a and 5b resolve frequency up to the Nyquist limit. For Figures 5c–and 5f a longer window of 64 s was used with the same 50% overlap to resolve down first to 0–1 Hz (Figures 4c and 4f) and then to 0–0.2 Hz (Figures 4e and 4f) including the 0.05 Hz range which is believed from statistical work to mark the transition between Alfvén waves and quasi-static FACs (e.g., Lühr et al., 2015).

4. Discussion

Despite the differences in residuals in magnetometer time series between Periods 1 and 2 (Figures 2 and 3), from the histograms of the impedance and phase differences during this period shown in Figures 4 and 5, a new picture emerges. All the time periods analyzed show characteristics which are qualitatively similar: at low frequencies, the calculated impedances are ~ 0.2 Ω for frequencies < 0.05 Hz, and with phase differences close to 0. The observed impedance increases with frequency with a sharply defined lower envelope edge which is expected to be related to the Pedersen conductance. This indicates that the perturbations characterizing the whole auroral zone crossing appear to be consistent with the Alfvén wave incidence, reflection, and interference paradigm with both the quasi-static and more rapidly varying field fluctuations being likely explained by the same physics. Crucially, from Figure 5 it can be seen that there does not appear to be a sharp discontinuity between the “quasi-static” and “Alfvén” regimes, but rather a smooth continuum in the impedance and phase functions in line with the theoretical predictions of Alfvén incidence, reflection, and interference models. As we discuss in more detail below, the behavior appears to be consistent with that expected for a continuum of reflected and interfering Alfvén waves, and specifically to be consistent with the response from a superposition of waves incident upon, and reflecting within, the ionospheric Alfvén resonator (see e.g., the model of Lysak, 1991, and references therein).

The impedance function as predicted by the model of Lysak (1991) for reflected Alfvén waves, is overplotted in Figures 4 and 5. The model can simulate frequency-dependent phase and impedance functions, assuming an Alfvén speed profile which increases exponentially with height above the ionospheric reflection layer. It also accounts for the peak in Alfvén speed which creates the cavity within which the ionospheric Alfvén resonator (e.g., Belyaev et al., 1990) operates.

The model was initialized with a representative ionospheric Alfvén speed of 70 km/s, a Pedersen conductance of 5 S, a scale height $h = 110$ km, and a height $z = 340$ km above the ionospheric reflection layer. The value of the Pedersen conductance was taken from the histogram in Figure 5e which shows a rapid decrease in data points at impedances below 0.2Ω . The scale height is taken as a representative value in the range for that local time during summer (Tulasi Ram et al., 2009). The height z is taken assuming that the waves are reflected from the *E*-layer (e.g., Fedorov et al., 2014) which is here assumed to be located at 110 km above Earth. Since Swarm A was at an altitude of ~ 450 km during the time of the event, this means the distance from Swarm to the assumed *E*-layer was 340 km. The Alfvén speed was selected empirically so as to best match the histogram data.

The model predicts an impedance equal to the inverse of the Pedersen conductance Σ_p at low frequencies and a zero phase difference between *E* and *B*. This is observed in the data presented here (e.g., in Figures 5e and 5f). At higher frequencies, the Lysak model predicts that the impedance function will be quasi-periodic oscillating between a lower and an upper bound determined by the Pedersen conductance, the ionospheric Alfvén speed, and the density scale height. Since the Swarm spacecraft are traveling across field lines, and each field line will likely have a different ionospheric Alfvén speed in traversing these different field lines, it is possible that this upper impedance limit will be expected to be smoothed out in the histograms of the data shown in Figures 4 and 5. This diffuse upper limit is also observed in the histograms for the highly correlated Period 1 (Figure 4b), the poorly correlated Period 2 (Figure 4e), and for the cumulative Period 3 (Figures 5a and 5c). In contrast, since the lower impedance envelope is largely controlled by Σ_p , then the envelopes of the histograms might be expected to have a sharper lower boundary, exactly as observed in Figures 4 and 5 for all three Periods 1, 2, and 3.

Meanwhile, the phase function is expected to have zero phase difference $\Delta\phi = 0$ for low frequencies (which is observed in Figure 5f), while at higher frequencies, it is expected to oscillate around $\Delta\phi = 0$ with the maximal deviation being between zero and $+90^\circ$ and -90° , dependent on the ratio of the Pedersen and Alfvén impedances. This range of phase behavior, albeit not a resolved oscillation as a function of frequency, is observed in this study for both the quasi-static (Figure 4e) and dynamic periods (Figure 4f) as well as for the whole crossing period (Figures 5b and 5d). It should be noted that the aforementioned phase and impedance function behavior is expected both in the case of a single reflection from the ionospheric *E*-layer and for the double reflection in the case of the IAR. The periodicity in the oscillation of both phase and impedance as a function of frequency is a function of distance from the reflecting boundary normalized to field aligned wavelength, which, of course, also depends on the Alfvén speed.

In the case of the IAR, there is also the development of a periodic impedance and phase between *E* and *B* as a function of frequency. However, in the IAR case the field-aligned wave numbers are quantized such that the periodicity of oscillation in frequency can be controlled by the global dispersion relation for the IAR, and not only by the local characteristics of phase development along the field from the ionospheric reflection height to the altitude of the satellite. In both cases, in the low frequency (i.e., long wavelength) limit then the phase difference between *E* and *B* becomes the same as that at the location of the ionospheric reflection, with the impedance being equal to $Z_p = 1/\Sigma_p$. As shown in Figures 4 and 5, the impedance observationally approaches an asymptotic low frequency limit of 0.2Ω , which seems reasonable for this location. For comparison the International Reference Ionosphere model gives an estimate for Z_p of $\sim 0.3 \Omega$. Indeed, a significant result from our work is an indication that low frequency analysis of electric and magnetic fields, such as presented here using Swarm, might be able to be used to diagnose the height integrated ionospheric Pedersen conductance.

Using the observed electron density from the Langmuir probe on Swarm A, and assuming an O+ plasma at these altitudes (e.g., Park et al., 2017), generates an Alfvén speed estimate of 639 km/s. Meanwhile, translating the assumed Alfvén speed at the ionospheric reflection point of 70 km/s to the Swarm height assuming the z and h values specified earlier gives an estimated Alfvén speed at Swarm height of 340 km/s. There are several

possible sources for this discrepancy between theoretically extrapolated Alfvén speed and Alfvén speed as measured by the Langmuir probe. First, the Langmuir probe is known to consistently underestimate density and thus overestimate Alfvén speed (e.g., Park et al., 2017, and references therein). Second, the scale height is a function of season, local time, and solar activity (e.g., Liu et al., 2006) and so may vary from event to event. Third, and potentially most significantly, the mass density profile between the altitude of Swarm A and the reflecting layer is likely not adequately captured by a simple scale height exponential and may well be more complex, especially between the *E* and *F* layers (e.g., Figure 10.3 in Gombosi, 1998). It is hoped that as work in this direction progresses onward from this proof-of-concept study, some of these challenges will be addressed and the agreement between the two values will improve.

As seen in the curves overplotted on the panels of Figure 4, periodic peaks in the impedance spectrum are generated at frequencies corresponding to near nodes in the electric field at the location of Swarm, the periodicity in frequency being determined by the Alfvén speed profile in the topside, and the maximum amplitude being determined by the nature of the wave interference at Swarm altitudes. An Alfvén speed of 70 km/s just above the ionosphere appears to generate oscillating impedance as a function of frequency whose envelope is in good agreement with the observations in Figure 4. Significantly, despite low-altitude uncertainty in the Alfvén speed profiles, the model for the IAR presented by Lysak (1991) initialized with parameters fitted from observations seems to reproduce the principal features of the observations, albeit driven by sources with varying frequencies in the frame of the Swarm satellites (mostly below 1 Hz for Period 1 and extending to higher frequencies during Period 2).

The asymmetry between the upper and lower cutoffs in the impedance histograms at higher frequencies presented in Figures 4 and 5 rejects the interpretation of the oscillations being caused by purely static field-aligned currents. In that case the expected impedance histogram would be a frequency-independent single value or a Gaussian with symmetric roll-offs in occurrence rate and a maximum corresponding to the Pedersen conductivity (e.g., Knudsen et al., 1992). Meanwhile, in the static FAC case the expected phase histogram would be a frequency-independent Gaussian centered sharply around 0° . Neither is observed here. However, the symmetric Gaussian-like distribution is observed in Figure 5e which concerns lower frequencies. This is also in line with model predictions as discussed above. Overall, we argue here that both the slowly varying and higher frequency magnetic fluctuations can all be explained by the same model of Alfvén wave incidence, reflection, and interference. Both for the slowly varying magnetic fields, which can be reliably used to estimate FAC even from single spacecraft, as well as those at higher frequencies, the impedance and phase profiles can be explained in the context of mutually interfering Alfvén waves and modeled using a generalized ionospheric Alfvén resonator model such as that presented by Lysak (1991).

This raises an intriguing possibility where instead of there being a divide between quasi-static FACs and dynamic Alfvén waves as has been proposed by the authors of previous studies (e.g., Lühr et al., 2015; Rother et al., 2007), it is possible that all of the dynamics observed during this auroral zone crossing may all be described in the context of Alfvén waves interacting with a reflecting ionospheric boundary (e.g., Song & Lysak, 2006). Attempts to differentiate between the quasi-static FAC and Alfvén waves phenomena using a scale separation of 150 km, and the related low-pass filter in the frame of Swarm, is an approach which has been used in the past, for example, in deriving the Swarm L2 FAC product (Ritter et al., 2013) and further in the work of Lühr et al. (2015). Based on the results presented here, such a separation at 150 km scale length seems to be rather arbitrary. Moreover, based on the results presented here, such filtering at periods corresponding in the frame of Swarm to this 150 km scale will act to exclude a portion of the auroral energy transport associated with such disturbances. Most significantly, while at higher frequencies the individual *E*- and *B*-field perturbations may time-average to zero, the downward Poynting flux associated with these disturbances/waves is a quadratic quantity which will not time-average to zero. Since the nonquasi-stationary regions are also associated with peak-to-peak values of magnetic field perturbation equal to or greater than those in the quasi-stationary regions, their energy content appears to be most likely significant. This will be a topic for further future analysis.

Interestingly, the region associated with the higher frequency disturbances also seems to occur in a region that AMPERE characterizes as a net downwards FAC region. Understanding why downward FACs appear, at least during this northward IMF case study, to produce finer-scale (nonstationary) magnetic fluctuations is also a subject of future work. Theoretically, feedback should be favored by large-scale

downward currents; however, recently, Sydorenko and Rankin (2017) have questioned the instability in a height-resolved ionosphere.

There are broadly speaking three proposed mechanisms for the creation of small scale structure within the auroral region. First, phase mixing has been discussed in the field-line resonance context by Mann, Wright, and Cally (1995) and in the IAR by Lysak and Song (2008) and seems to be the most universal mechanism, requiring only gradients perpendicular to the field and second, the feedback mechanism as discussed in Lysak (1991) and, for example, Streltsov and Lotko (2008), which favors low ionospheric conductance. Finally, a third candidate process would involve nonlinear coupling (e.g., Chaston et al., 2008); however, in the auroral zone several of the underlying assumptions for that process would be violated (Lysak & Song, 2008). Nevertheless, all three candidate processes can produce fine-scale structuring in Poynting flux and could account for the observations seen in this study.

Overall, based on the analysis presented here, it appears that both the low and higher frequency perturbations can be interpreted within the framework of Alfvén waves within the IAR (a single reflection from the ionosphere being a special case of the general IAR framework). The only differences between quasi-stationary and nonquasi-stationary behavior can then be interpreted as being due only to the wave scale lengths and distance from the reflecting layer. Of course, in this context the more quasi-static behavior (longer period, longer wavelength waves) can also be naturally interpreted as slower time varying disturbances. Since Alfvén wave propagation is required to establish or change a FAC, such an Alfvén wave model provides a natural connection to the FAC distributions in dynamic MIC. Indeed, within this paradigm even quasi-static FAC might be reasonably interpreted as very low frequency ($\omega \rightarrow 0$) Alfvén waves.

Acknowledgments

This work was supported in part by ESA contract 4000114090 (Swarm Investigation of the Role of High-Frequency (0.1–5 Hz) ULF Waves in Magnetosphere-Ionosphere Coupling) Swarm + Support to Science Element. I. R. Mann is supported by a discovery grant from Canadian NSERC. This work was also partially supported by the Canadian Space Agency Geospace Observatory (GO) Canada Science and Applications program. C. Forsyth is supported by a Natural Environment Research Council Independent Research Fellowship (NE/N014480/1). I. J. Rae is supported in part by a Science and Technology Facilities Council Grant (STFC) ST/N000722/1 and NERC grants NE/L007495/1 and NE/P017150/1. D. M. Miles was supported by an NSERC PGSD graduate scholarship and by funding from the Canadian Space Agency. R. L. Lysak is supported by NSF grant AGS-1558134. The authors thank Johnathan Burchill for assistance with the 16 s^{-1} TII data. The authors thank the AMPERE team and the AMPERE Science Center for providing the Iridium-derived data products. The authors would like to separately thank Haje Korth for assistance with the AMPERE visualization toolkit. The ESA Swarm data can be obtained from the ESA server at swarm-diss.eo.esa.int. AMPERE data can be downloaded from <http://ampere.jhuapl.edu>. Geomagnetic conditions and L1 information used to make Figure 1a can be found on <https://omniweb.gsfc.nasa.gov>. The CARISMA ground magnetometer data used to make Figure 1c can be obtained from <http://www.carisma.ca>.

5. Conclusions

1. An analysis of the magnetic field data for a FAC system crossed by Swarm A and C during northward IMF conditions revealed evidence for ~ 100 nT large-amplitude nonstationary magnetic structures which evolve on 10 s timescales.
2. Analysis of the independent measurements of the electric and magnetic fields reveals phase differences which are a function of frequency, rather than the zero phase difference expected for static structures. This is indicative of the control of these disturbances by the incidence, ionospheric reflection, and interference of Alfvén waves.
3. An analysis of the amplitude ratio and cross phase of the E - and B -field data reveals a continuum of fluctuations spanning a frequency range of up to at least 8 Hz, and with phase and impedance characteristics consistent with a framework of energy transfer in the coupled magnetosphere-ionosphere system arising from the incidence, reflection, partial absorption, and interference of Alfvén waves. The possibility of interspacecraft variation at higher frequencies being caused by azimuthally localized fine-scale quasi-static currents is examined and rejected as inconsistent with the synchronous E - and B -field observations available from Swarm A.
4. The wave analysis presented here also provides a potential method for remote sensing ionospheric Pedersen conductance based on the low-frequency behavior of the combined E - and B -field measurements.
5. Analysis of the large amplitude magnetic signatures, together with coincident electric fields, is consistent with the conclusion that Alfvén wave dynamics are an integral and important part of the coupled magnetosphere-ionosphere system. Filtering out fine spatial scale magnetic perturbations based on (what we argue is an arbitrary) scale of 150 km as is often done (e.g., Lühr et al., 2015; Ritter et al., 2013) seems, on the basis of the results presented here, to obscure important physical processes—especially those associated with Alfvén waves which are active in magnetosphere-ionosphere coupling.

References

- Anderson, B. J., Takahashi, K., & Toth, B. A. (2000). Sensing global Birkeland currents with Iridium® engineering magnetometer data. *Geophysical Research Letters*, 27, 4045–4048. <https://doi.org/10.1029/2000GL000094>
- Anderson, B. J., Takahashi, K., Kamei, T., Waters, C. L., & Toth, B. A. (2002). Birkeland current system key parameters derived from Iridium observations: Method and initial validation results. *Journal of Geophysical Research*, 107(A6), 1079. <https://doi.org/10.1029/2001JA000080>
- Belyaev, P. P., Polyakov, S. V., Rapoport, V. O., & Trakhtengert, V. Y. (1990). The ionospheric Alfvén resonator. *Journal of Atmospheric and Terrestrial Physics*, 52(9), 781–788. [https://doi.org/10.1016/0021-9169\(90\)90010-K](https://doi.org/10.1016/0021-9169(90)90010-K)

- Chaston, C. C., Salem, C., Bonnell, J. W., Carlson, C. W., Ergun, R. E., Strangeway, R. J., & McFadden, J. P. (2008). The turbulent Alfvénic aurora. *Physical Review Letters*, *100*, 175003. <https://doi.org/10.1103/PhysRevLett.100.175003>
- Cowley, S. W. H. (2000). Magnetosphere-ionosphere interactions: A tutorial review. In S.-I. Ohtani, R. Fujii, M. Hesse, & R. L. Lysak (Eds.), *Magnetospheric current systems* (p. 91). Washington, DC: American Geophysical Union. <https://doi.org/10.1029/GM118p0091>
- Fedorov, E., Schekotov, A., Hobara, Y., Nakamura, R., Yagova, N., & Hayakawa, M. (2014). The origin of spectral resonance structures of the ionospheric Alfvén resonator. Single high-altitude reflection or resonant cavity excitation? *Journal of Geophysical Research: Space Physics*, *119*, 3117–3129. <https://doi.org/10.1002/2013JA019428>
- Forsyth, C., Rae, I. J., Mann, I. R., & Pakhotin, I. P. (2017). Identifying intervals of temporally invariant field-aligned currents from Swarm: Assessing the validity of single-spacecraft methods. *Journal of Geophysical Research: Space Physics*, *122*, 3411–3419. <https://doi.org/10.1002/2016JA023708>
- Foster, J. C., St-Maurice, J.-P., & Abreu, V. J. (1983). Joule heating at high latitudes. *Journal of Geophysical Research*, *88*, 4885–4896. <https://doi.org/10.1029/JA088iA06p04885>
- Friis-Christensen, E., Lühr, H., Knudsen, D., & Haagmans, R. (2008). Swarm—An Earth observation mission investigating geospace. *Advances in Space Research*, *41*, 210–216. <https://doi.org/10.1016/j.asr.2006.10.008>
- Gjerloev, J. W., Ohtani, S., Iijima, T., Anderson, B., Slavin, J., & Le, G. (2011). Characteristics of the terrestrial field-aligned current system. *Annales Geophysicae*, *29*, 1713–1729. <https://doi.org/10.5194/angeo-29-1713-2011>
- Gombosi, T. (1998). *Physics of the Space Environment* (p. 178). Cambridge University Press. <https://doi.org/10.1017/CBO9780511529474>
- Green, D. L., Waters, C. L., Anderson, B. J., Korth, H., & Barnes, R. J. (2006). Comparison of large-scale Birkeland currents determined from iridium and SuperDARN data. *Annales Geophysicae*, *24*(3), 941–959.
- Grzesiak, M. (2000). Ionospheric Alfvén resonator as seen by Freja satellite. *Geophysical Research Letters*, *27*, 923–926. <https://doi.org/10.1029/1999GL010747>
- Hasunuma, T., Nagatsuma, T., Kataoka, R., Takahashi, Y., Fukunishi, H., Matsuoka, A., & Kumamoto, A. (2008). Statistical study of polar distribution of mesoscale field-aligned currents. *Journal of Geophysical Research*, *113*, A12214. <https://doi.org/10.1029/2008JA013358>
- Hoffman, R. A., Sugiura, M., Maynard, N. C., Candey, R. M., Craven, J. D., & Frank, L. A. (1988). Electrodynamical patterns in the polar region during periods of extreme magnetic quiescence. *Journal of Geophysical Research*, *93*, 14,515–14,541. <https://doi.org/10.1029/JA093iA12p14515>
- Iijima, T., & Potemra, T. A. (1976). The amplitude distribution of field-aligned currents at northern high latitudes observed by Triad. *Journal of Geophysical Research*, *81*, 2165–2174. <https://doi.org/10.1029/JA081i013p02165>
- Iijima, T., & Potemra, T. A. (1978). Large-scale characteristics of field-aligned currents associated with substorms. *Journal of Geophysical Research*, *83*, 599–615. <https://doi.org/10.1029/JA083iA02p00599>
- Ishii, M., Sugiura, M., Iyemori, T., & Slavin, J. A. (1992). Correlation between magnetic and electric field perturbations in the field-aligned current regions deduced from DE 2 observations. *Journal of Geophysical Research*, *97*, 13,877–13,887. <https://doi.org/10.1029/92JA00110>
- King, J. H., & Papitashvili, N. E. (2005). Solar wind spatial scales in and comparisons of hourly Wind and ACE plasma and magnetic field data. *Journal of Geophysical Research*, *110*, A02104. <https://doi.org/10.1029/2004JA010649>
- Knudsen, D. J., Kelley, M. C., Earle, G. D., Vickrey, J. F., & Boehm, M. (1990). Distinguishing Alfvén waves from quasi-static field structures associated with the discrete aurora: Sounding rocket and HILAT satellite measurements. *Geophysical Research Letters*, *17*, 921–924. <https://doi.org/10.1029/GL017i007p00921>
- Knudsen, D. J., Kelley, M. C., & Vickrey, J. F. (1992). Alfvén waves in the auroral ionosphere: A numerical model compared with measurements. *Journal of Geophysical Research*, *97*, 77–90. <https://doi.org/10.1029/91JA02300>
- Knudsen, D. J., Burchill, J. K., Buchert, S. C., Eriksson, A. I., Gill, R., Wahlund, J.-E., ... Moffat, B. (2017). Thermal ion imagers and Langmuir probes in the Swarm electric field instruments. *Journal of Geophysical Research: Space Physics*, *122*, 2655–2673. <https://doi.org/10.1002/2016JA022571>
- Liu, L., Wan, W., & Ning, B. (2006). A study of the ionogram derived effective scale height around the ionospheric hmF2. *Annales de Geophysique*, *24*, 851–860. <https://doi.org/10.5194/angeo-24-851-2006>
- Lu, G., Baker, D. N., McPherron, R. L., Farrugia, C. J., Lummerzheim, D., Ruohoniemi, J. M., ... Hayashi, K. (1998). Global energy deposition during the January 1997 magnetic cloud event. *Journal of Geophysical Research*, *103*, 11,685–11,694. <https://doi.org/10.1029/98JA00897>
- Lühr, H., Park, J., Gjerloev, J. W., Rauberg, J., Michaelis, I., Merayo, J. M. G., & Brauer, P. (2015). Field-aligned currents' scale analysis performed with the Swarm constellation. *Geophysical Research Letters*, *42*, 1–8. <https://doi.org/10.1002/2014GL02453>
- Lysak, R. L. (1991). Feedback instability of the ionospheric resonant cavity. *Journal of Geophysical Research*, *96*, 1553–1568. <https://doi.org/10.1029/90JA02154>
- Lysak, R. L., & Song, Y. (2008). Propagation of kinetic Alfvén waves in the ionospheric Alfvén resonator in the presence of density cavities. *Geophysical Research Letters*, *35*, L20101. <https://doi.org/10.1029/2008GL035728>
- Mann, I. R., Wright, A. N., & Cally, P. S. (1995). Coupling of magnetospheric cavity modes to field line resonances: A study of resonance widths. *Journal of Geophysical Research*, *100*, 19,441–19,456. <https://doi.org/10.1029/95JA00820>
- Mann, I. R., Milling, D. K., Rae, I. J., Ozeke, L. G., Kale, A., Kale, Z. C., ... Singer, H. J. (2008). The upgraded CARISMA magnetometer array in the THEMIS era. *Space Science Reviews*, *141*(1-4), 413–451. <https://doi.org/10.1007/s11214-008-9457-6>
- Miles, D. M., Mann, I. R., Ciurzynski, M., Barona, D., Narod, B. B., Bennet, J. R., ... Milling, D. K. (2016). A miniature, low-power scientific fluxgate magnetometer: A stepping-stone to cubesatellite constellation missions. *Journal of Geophysical Research: Space Physics*, *121*, 11,839–11,860. <https://doi.org/10.1002/2016JA023147>
- Murphy, K. R., Mann, I. R., Rae, I. J., Waters, C. L., Anderson, B. J., Milling, D. K., ... Korth, H. (2012). Reduction in field-aligned currents preceding and local to auroral substorm onset. *Geophysical Research Letters*, *39*, L15106. <https://doi.org/10.1029/2012GL052798>
- Murphy, K. R., Mann, I. R., Rae, I. J., Waters, C. L., Frey, H. U., Kale, A., ... Korth, H. (2013). The detailed spatial structure of field-aligned currents comprising the substorm current wedge. *Journal of Geophysical Research: Space Physics*, *118*, 7714–7727. <https://doi.org/10.1002/2013JA018979>
- Newell, P. T., Xu, D., Meng, C. I., & Kivelson, M. G. (1997). Dynamical polar cap: A unifying approach. *Journal of Geophysical Research*, *102*, 127–139. <https://doi.org/10.1029/96JA03045>
- Ohtani, S., Blomberg, L. G., Newell, P. T., Yamauchi, M., Potemra, T. A., & Zanetti, L. J. (1996). Altitudinal comparison of dayside field-aligned current signatures by Viking and DMSP-F7: Intermediate-scale field-aligned current systems. *Journal of Geophysical Research*, *101*, 15,297–15,310. <https://doi.org/10.1029/96JA00686>
- Park, J., Lühr, H., Knudsen, D. J., Burchill, J. K., & Kwak, Y.-S. (2017). Alfvén waves in the auroral region, their Poynting flux, and reflection coefficient as estimated from Swarm observations. *Journal of Geophysical Research: Space Physics*, *122*, 2345–2360. <https://doi.org/10.1002/2016JA023527>

- Peria, W. J., Carlson, C. W., Ergun, R. E., McFadden, J. P., Bonnell, J., Elphic, R. C., & Strangeway, R. J. (2000). Characteristics of field-aligned currents near the auroral acceleration region: FAST observations. In S.-I. Ohtani, R. Fujii, M. Hesse, & R. L. Lysak (Eds.), *Magnetospheric current systems* (p. 181). Washington, DC: American Geophysical Union.
- Ritter, P., Lühr, H., & Rauberg, J. (2013). Determining field-aligned currents with the Swarm constellation mission. *Earth, Planets and Space*, *65*(11), 1285–1294. <https://doi.org/10.5047/eps.2013.09.006>
- Rother, M., Schlegel, K., & Lühr, H. (2007). CHAMP observation of intense kilometer-scale field-aligned currents, evidence for an ionospheric Alfvén resonator. *Annales Geophysicae*, *25*(7), 1603–1615. <https://doi.org/10.5194/angeo-25-1603-2007>.
- Song, Y., & Lysak, R. L. (2006). The displacement current and the generation of parallel electric fields. *Physical Review Letters*, *96*, 145002. <https://doi.org/10.1103/PhysRevLett.96.145002>
- Streltsov, A. V., & Lotko, W. (2008). Coupling between density structures, electromagnetic waves and ionospheric feedback in the auroral zone. *Journal of Geophysical Research*, *113*, A05212. <https://doi.org/10.1029/2007JA012594>
- Sugiura, M., Maynard, N. C., Farthing, W. H., Heppner, J. P., Ledley, B. G., & Cahill, L. J. (1982). Initial results on the correlation between the magnetic and electric fields observed from the DE-2 satellite in the field-aligned current regions. *Geophysical Research Letters*, *9*, 985–988. <https://doi.org/10.1029/GL009i009p00985>
- Sydorenko, D., & Rankin, R. (2017). The stabilizing effect of collision-induced velocity shear on the ionospheric feedback instability in Earth's magnetosphere. *Geophysical Research Letters*, *44*, 6534–6542. <https://doi.org/10.1002/2017GL073415>
- Tulasi Ram, S., Su, S.-Y., Liu, C. H., Reinisch, B. W., & McKinnell, L.-A. (2009). Topside ionospheric effective scale heights (HT) derived with ROCSAT-1 and ground-based ionosonde observations at equatorial and midlatitude stations. *Journal of Geophysical Research*, *114*, A10309. <https://doi.org/10.1029/2009JA014485>
- Waters, C. L., Anderson, B. J., & Liou, K. (2001). Estimation of global field aligned currents using the iridium system magnetometer data. *Geophysical Research Letters*, *28*, 2165–2168. <https://doi.org/10.1029/2000GL012725>
- Woodroffe, J. R., & Lysak, R. L. (2012). Ultra-low frequency wave coupling in the ionospheric Alfvén resonator: Characteristics and implications for the interpretation of ground magnetic fields. *Journal of Geophysical Research*, *117*, A03223. <https://doi.org/10.1029/2011JA017057>
- Wright, A. N. (1996). Transfer of magnetosheath momentum and energy to the ionosphere along open field lines. *Journal of Geophysical Research*, *101*, 13,169–13,178. <https://doi.org/10.1029/96JA00541>